NANO LETTERS

2004
Vol. 4, No. 6
1085−1088

Plasmonic Nanolithography

Werayut Srituravanich, Nicholas Fang, Cheng Sun, Qi Luo, and Xiang Zhang*

Mechanical & Aerospace Engineering Department,
University of California at Los Angeles, Los Angeles, California 90095

Received March 17, 2004; Revised Manuscript Received May 5, 2004

ABSTRACT

In this paper, we demonstrate high-density nanolithography by utilizing surface plasmons (SPs). SPs are excited on an aluminum substrate perforated with 2-D hole arrays using a near UV light source in order to resolve sub-wavelength features with high transmission. Our lithography experiments using a 365 nm wavelength light source demonstrate 90 nm dot array patterns on a 170 nm period, well beyond the diffraction limit of far-field optical lithography. In far-field transmission measurements, strong UV light transmission and the wavelength-dependent transmission are observed, which confirms the contribution of SPs. Furthermore, an exposure with larger spacing between the mask and photoresist has been explored for potential noncontact lithography.

There is a growing interest in developing nanolithography to fabricate nanoscale devices for nanotechnology applications. Several methods such as near-field optical lithography,[1−4] electron-beam lithography,[5] imprint lithography,[6−8] scanning probe lithography,[9,10] and dip-pen lithography[11,12] have been developed in order to achieve nanometer-scale features. Among them, imprint lithography and optical lithography are very attractive due to the high throughput for mass fabrication. Imprint lithography can generate nanometer-scale features by stamping a template on a thin polymer film. However, the leveling of the imprint template and the substrate during the printing process, which determines the uniformity of the imprint result, is a challenging issue of this method.[6−8] On the other hand, photolithography has been a major fabrication method in the integrated circuit (IC) and semiconductor industries over the past several decades. Advanced deep UV photolithography can now offer sub-100 nm resolution, yet the minimum feature size and spacing between patterns are determined by the diffraction limit of light. Its derivative technologies such as evanescent near field lithography,[1] near field interference lithography,[2] and phase-shifting mask lithography[3] were developed to overcome the diffraction limit. For example, evanescent near-field lithography using a contact mask can generate a 1D grating of 70 nm lines on a 140 nm period.[1] However, the evanescent field decays rapidly through the aperture, thus attenuating the transmission intensity at the exit plane and limiting the exposed distance to the scale of a few tens of nanometers from the mask. Near field interference photolithography using embedded-amplitude masks can generate a feature size down to 1/6 of the aperture size in the mask, and a sub-50 nm pattern has been successfully obtained by using a 220 nm wavelength light source.[2] However, to generate sub-wavelength features from apertures much smaller than the exposing wavelength, the critical concerns are extremely low transmission through the apertures, limitation of the exposing distance away from the mask, and poor contrast.

The potential of using surface plasmons (SPs) to manipulate light in the sub-wavelength regime is of interest due to their potential in sub-wavelength lithography, data storage, microscopy, and biophotonics.[13] The recent discovery of extraordinary transmission through sub-wavelength hole arrays on an opaque metal film has stimulated extensive interest in SPs among the scientific community.[14−18] The observed far-field transmission through a silver hole array in the infrared and visible regions can be enhanced by orders of magnitude compared to that of a single hole.[14] This unusual enhancement is attributed to the excitation of SPs on the metal surface which dramatically enhances the optical throughput via the sub-wavelength aperture.

The interaction of light and SPs is described by the SP dispersion relation (the frequency-dependent SP wavevector, k_{SP})[19] in eq 1:

$$k_{SP} = k_0\sqrt{\frac{\epsilon_d\epsilon_m}{\epsilon_d + \epsilon_m}} \tag{1}$$

where k_0 is the wavevector of light in vacuum, ϵ_m and ϵ_d are dielectric constants of a metal and a surrounding dielectric material, respectively. According to the SP dispersion curve as shown in Figure 1, the wavelength of the excited SPs is shorter compared to the wavelength of the excitation light at the same frequency, therefore smaller features are expected in the lithography. Generally light cannot excite SPs on the metal surface directly due to the momentum mismatch between the light waves and the waves of the SPs. However, by matching these momentums, typically by using a rough

* Corresponding author. E-mail: xiang@seas.ucla.edu

10.1021/nl049573q CCC: $27.50 © 2004 American Chemical Society
Published on Web 05/19/2004

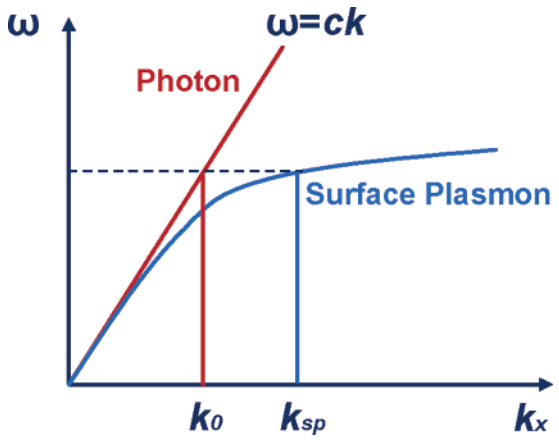

Figure 1. Schematic drawing of the surface plasmon dispersion curve. At the same frequency, surface plasmons display a shorter modal wavelength compared to that of free space photons, thus allowing sub-wavelength lithography.

surface, grating coupler, or attenuated total reflection (ATR) coupler, light can be converted into SPs and vice versa. For instance, a 2D square array of holes can be treated as a 2D grating coupler. By selecting a proper periodicity of hole array and a proper dielectric constant of the medium surrounding the metal substrate, light can excite SP waves on the incident side, and these SP waves can be resonantly coupled through the periodic hole array to the other side of the metal.[14,16] If the dielectric constant of the dielectric layers match on both sides of the metal layer, the SP waves on the exit plane scattered on the hole array will be converted back into the light waves. In the case of a normal incident light on a 2D hole array, the light wavelengths that excite the SP resonance mode are given by[16]

$$\lambda(i,j) = \frac{a}{\sqrt{i^2 + j^2}} \sqrt{\frac{\epsilon_d \epsilon_m}{\epsilon_d + \epsilon_m}} \qquad (2)$$

where λ is the light wavelength in vacuum, a is the hole array period, i and j are mode indices.

The remarkable transmission of the SP waves through the sub-wavelength plasmonic masks at UV wavelength has a potential to pattern nanoscale features using conventional near UV light sources. In this paper, we demonstrate a novel UV nanolithography by utilizing SPs transmitted through sub-wavelength 2D hole array masks.

The configuration of the SP optical lithography is illustrated in Figure 2A. A plasmonic mask designed for lithography in the UV range is composed of an aluminum layer perforated with 2D periodic hole arrays and two surrounding dielectric layers on each side. Aluminum is chosen since it can excite the SPs in the UV range.[19] Quartz is employed as the mask support substrate, and the spacer layer of poly(methyl methacrylate) (495-PMMA, MicroChem) as the matching dielectric material because of their transparency to the UV light and comparable dielectric constants (2.18 and 2.30) at the exposure wavelength of 365 nm (*i*-line). As a proof of the concept, a negative near-UV

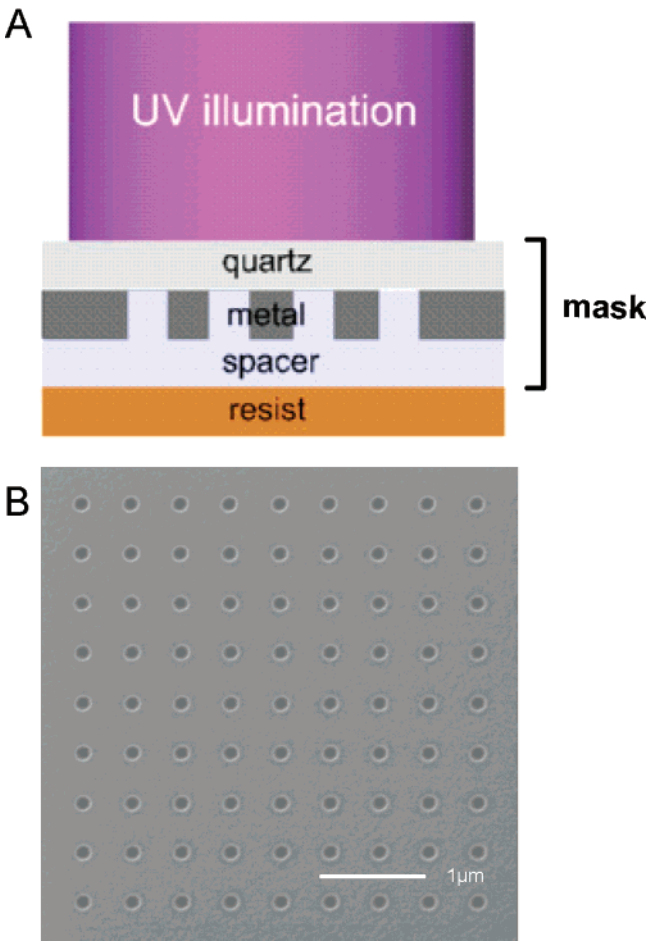

Figure 2. (A) Schematic drawing of the surface plasmon optical lithography. Focused ion beam is used to fabricate 2D hole arrays on aluminum substrates. PMMA is chosen as the spacer layer to match the dielectric constant of the quartz substrate. (B) FIB image of an hole array mask with hole size of 160 nm and period of 500 nm.

photoresist (SU-8) is directly spun on the top of the spacer layer and polymerized on the mask in order to eliminate the gap variation between the mask and the photoresist in the lithography process.

In our lithography experiment, the plasmonic mask is prepared as follows (Figure 2B): 40 nm diameter hole arrays with the period of 170, 220, and 250 nm are fabricated on an 80 nm thick aluminum film by focused ion beam milling (FIB, FEI Strata 201 XP). The 220 nm period corresponds to (1,0) and (0,1) resonance modes as calculated from eq 2 using the dielectric constant of aluminum from the literature.[20] Subsequently, a 30 nm thick spacer layer of PMMA is spun on the top of the patterned aluminum film, and next the photoresist (SU-8) is spun on the spacer layer. Exposure is performed using a filtered mercury lamp with a radiation peak at 365 nm. After the development, the topography of exposure features is characterized by atomic force microscopy (AFM, Dimension 3100, Digital Instruments).

The AFM image in Figure 3A is an exposure result obtained from the 170 nm period die. Features as small as 90 nm (equivalent to $\sim\lambda/4$, where λ is the exposure light wavelength) have been achieved. It should be emphasized

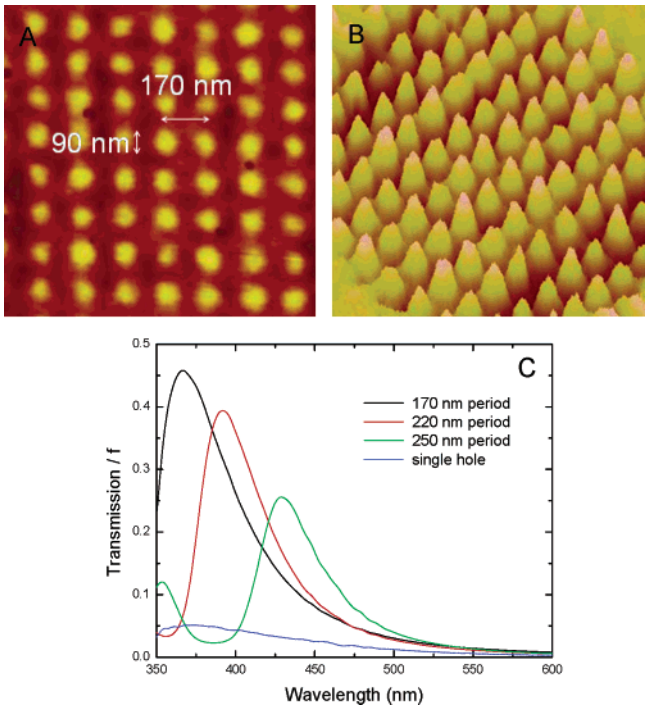

Figure 3. (A) AFM image of a pattern with 90 nm features on a 170 nm period obtained by surface plasmon lithography. The mask is an array of 40 nm holes on a 170 nm period. The spacer layer thickness is 30 nm, and the exposure dose of 72 mJ/cm^2. (B) 3D topography image of (A). (C) Spectrum measurement of far-field transmission normalized to the hole area (f) through hole arrays of three different samples; 170, 220, and 250 nm period compared to that of single hole.

that the pattern period is smaller than half of the exposure light wavelength, far beyond the diffraction limit of far-field lithography. In addition, the conventional contact lithography at this hole size of 40 nm (equivalent to $\sim\lambda/9$) suffers severe attenuation of transmission and exposure would become impractically long. In contrast, we find the optimal exposure time is only 9 s, corresponding to an exposure dose of 72 mJ/cm^2 at the mask. Surprisingly, this is comparable to a typical exposure dose used in conventional lithography with larger features, which implies a strong near-field transmission enhancement due to SPs. The height of the exposure pattern is $\sim$10 nm as shown in Figure 3B. It should be noted that smaller features can be achieved by reducing the spacer layer thickness, which opens up a possibility of high resolution and density nanolithography with high transmittance using a conventional light source without the complicated setup and vacuum requirement such as in the extreme UV lithography.

For a qualitative comparison, we measured far-field transmission spectra of the samples used in the lithography experiment. The transmission of a broadband light source is collected through an oil immersion lens (NA = 1.3) to a spectrometer. The matching oil used in the measurement has the dielectric constant of 2.30. Figure 3C shows the transmission normalized to the hole area (f) of the hole arrays compared to that of a single hole. The observed transmission spectra strongly depend on the wavelength and the period of the hole array, which confirms the role of SPs. For the wavelength of 365 nm as the exposure light wavelength in the previous experiment, the transmission peak is observed on the die of the 170 nm period instead of the 220 nm period as predicted by eq 2. This shift of the peak from the predicted value can be attributed to the deviation of optical properties of our evaporated aluminum film compared to the literature.[20] It has been reported that variations in the refractive indices (n,k) of evaporated films can arise from a surface oxide layer, residual gas in the film, surface roughness, and film morphology based on the evaporation conditions.[21] The peak shift due to these factors can be several tens of nanometers, which is consistent with our measurement results.

In addition, we explored the plasmonic lithography with a set of different periodicity, and the results are shown in Figure 4. Figure 4A, 4B, and 4C illustrate the lithographic results from the hole arrays with periods of 470, 420, and 380 nm, respectively, with an exposure dose of 100 mJ/cm^2. The masks constitute hole arrays with hole size of 100 nm and a spacer layer (PMMA) thickness of 50 nm. The exposure results from these three dies indicate distinct near-field intensity profiles due to the characteristic of SP-enhanced transmission at different periods. It is noted that the result in Figure 4c is due to the overexposure and is possibly distorted during the development and hard bake processes. This can be improved by the optimization of the post bake, development, and hard bake processes.

Finally, an exposure condition with larger spacing between the mask and the photoresist has been investigated. This is significant, as a longer exposure distance is desirable for noncontact lithography. Figure 5A shows an AFM image of the exposure pattern on the photoresist with an exposure dose of 200mJ/cm^2, and Figure 5B shows its cross-sectional image. The mask consists of a hole array with hole size of 160 nm, period of 500 nm, and spacer layer thickness of 150 nm. The cross-sectional image shows the exposure patterns as small as 120 nm measured at half modulation, and the average modulation height is about 50 nm. The demonstration of the well-confined pattern at large spacing implies the potential in noncontact plasmonic lithography.

In conclusion, a novel plasmonic photolithography using periodic hole array masks has been demonstrated. This technique utilizes near UV light to excite SPs on a metal substrate in order to enhance the transmission through sub-wavelength periodic apertures with effectively shorter wavelengths compared to the excitation light wavelength. A sub-100 nm dot array pattern on a 170 nm period has been successfully obtained using an exposure radiation of 365 nm wavelength. Far field transmission spectra measurement of the designed structures shows strongly enhanced transmission in the UV range, which opens the possibility of lithography using the apertures much smaller than the exposing wavelength. We also investigated the effect of changing the hole array period and the spacer thickness. It shows promise in high resolution, high density, and strong transmission optical lithography, which can be used to fabricate periodic structures for potential biosensing, photonic crystals, and high density patterned magnetic storage. The concept of plasmonic lithography applies not only to periodic structures but also

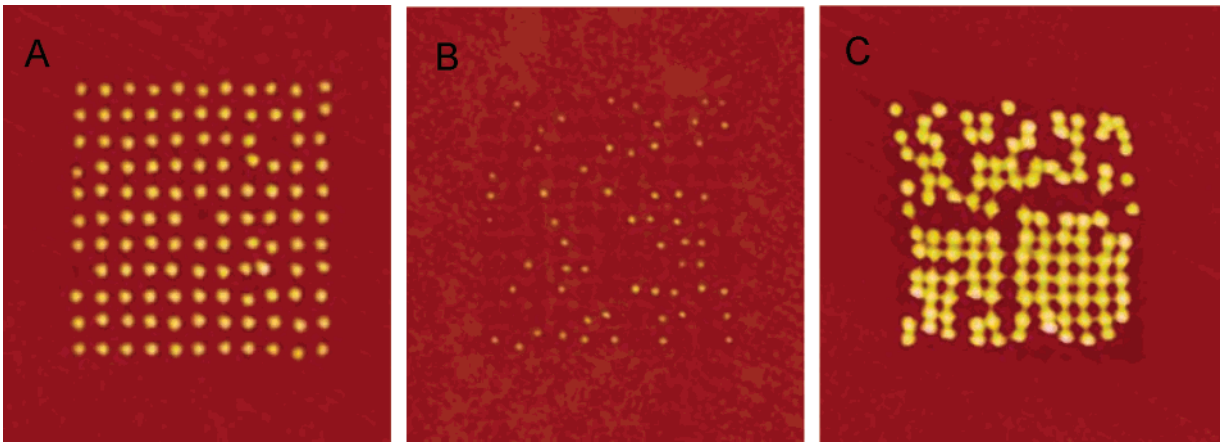

Figure 4. AFM images of exposure patterns with the period of (A) 470 nm, (B) 420 nm, and (C) 380 nm, with the hole size of 100 nm, the aluminum film thickness of 80 nm, the spacer layer thickness of 50 nm, and the exposure dose of 100 mJ/cm^2. It is noted that the deformation of photoresist in the 380 nm period die may have originated from the development and subsequent hard bake processes.

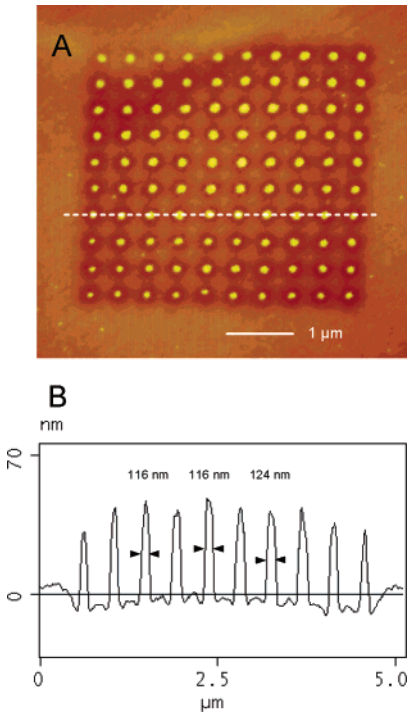

Figure 5. (A) AFM image of a pattern obtained at large spacing (150 nm above the mask), with the mask period of 500 nm, the hole size of 160 nm, the spacer layer thickness of 150 nm, and the exposure dose of 200 mJ/cm^2. (B) Cross-sectional image along the white line shown in (A).

to arbitrary shapes. Currently, we are developing methods to achieve fully parallel arbitrary patterning plasmonic lithography.

Acknowledgment. The authors are grateful to Dr. Qihuo Wei, Dr. Stephane Durant, Fujino Makoto, and Muralidhar Ambati for the helpful discussions. This work was supported by MURI (Grant # N00014-01-1-0803), NSF on Nanoscale Science and Engineering Center (NSEC) (Grant # DMI-0327077), and NSF (Grant # DMI-0218273).

References

(1) Alkaisi, M. M.; Blaikie, R. J.; Mcnab, S. J. *Micro. Eng.* **2000**, *53*, 237−240.
(2) Goodberlet, J. G.; Kavak, H. *Appl. Phys. Lett.* **2002**, *81*, 1315−1317.
(3) Kunz, R. R.; Rothschild, M.; Yeung, M. S. *J. Vac. Sci. Technol. B* **2003**, *21*, 78−81.
(4) Schmid, H.; Biebuyck, H.; Michel, B.; Martin, O. J. F. *Appl. Phys. Lett.* **1998**, *72*, 2379−2381.
(5) Dhaliwal, R. S.; Enichen, W. A.; Golldaday, S. D.; Gordon, M. S.; Kendall, R. A.; Lieberman, J. E.; Pfeiffer, H. C.; Pinckney, D. J.; Robinson, C. F.; Rockrohr, J. D.; Stickel, W.; Tressler, E. V. *IBM J. Res. Dev.* **2001**, *45*, 615−638.
(6) Chou, S. Y.; Krauss, P. R.; Renstrom, P. J. *Science* **1996**, *272*, 85−87.
(7) Colburn, M.; Bailey, T.; Choi, B. J.; Ekerdt, J. G.; Sreenivasan, S. V.; Willson, C. G. *Solid State Technol.* **2001**, *44*, 67−78.
(8) McAlpine, M. C.; Friedman, R. S.; Lieber, C. M. *Nano Lett.* **2003**, *3*, 443−445.
(9) Cooper, E. B.; Manalis, S. R.; Fang, H.; Dai, H.; Matsumoto, K.; Minne, S. C.; Hunt, T.; Quate, C. F. *Appl. Phys. Lett.* **1999**, *75*, 3566−3568.
(10) Yin, X.; Fang, N.; Zhang, X.; Martini, I. B.; Schwartz, B. J. *Appl. Phys. Lett.* **2002**, *81*, 3663−3665.
(11) Piner, R. D.; Zhu, J.; Xu, F.; Hong, S.; Mirkin, C. A. *Science* **1999**, *283*, 661−663.
(12) Zhang, H.; Chung, S.-W.; Mirkin, C. A. *Nano Lett.* **2003**, *3*, 43−45.
(13) Barnes, W. L.; Dereux, A.; Ebbesen, T. W. *Nature (London)* **2003**, 424, 824−830.
(14) Ebbesen, T. W.; Lezec, H. J.; Ghaemi, H. F.; Thio, T.; Wolff, P. A. *Nature (London)* **1998**, *391*, 667−669.
(15) Thio, T.; Ghaemi, H. F.; Lezec, H. J.; Wolff, P. A.; Ebbesen, T. W. *JOSA B* **1999**, *16*, 1743−1748.
(16) Krishnan, A.; Thio, T.; Kim, T. J.; Lezec, H. J.; Ebbesen, T. W.; Wolff, P. A.; Pendry, J.; Martin-Moreno, L.; Garcia-Vidal, F. J. *Opt. Commun.* **2001**, *200*, 1−7.
(17) Dogariu A.; Nahata, A.; Linke, R. A.; Wang, L. J.; Trebino, R. *Appl. Phys. B* **2002**, *74*, S69−S73.
(18) Salomon, L.; Grillot, F.; Zayats, A. V.; de Fornel, F. *Phys. Rev. Lett.* **2001**, *86*, 1110−1113.
(19) Raether, H. *Surface Plasmons on Smooth and Rough Surfaces and on Gratings*; Springer: Berlin, 1988; pp 25−30.
(20) Weaver, J. H.; Frederkse, H. P. R. *CRC Handbook of Chemistry and Physics*, 83rd ed.; CRC Press, LLC: Boca Raton, 2002; section 12, pp 133−156.
(21) Palik, E. D. *Handbook of Optical Constants*; Academic Press: New York, 1985; pp 369−391. Note that the refractive indices of films evaporated in higher vacuum (~10^{-5}−10^{-6} Torr) tend to be slightly smaller, resulting in the shift toward longer wavelength.

NL049573Q